Revised version, submitted to *Nature*, Nov. 2004

Strong polarization enhancement in asymmetric three-component ferroelectric superlattices

Ho Nyung Lee, Hans M. Christen, Matthew F. Chisholm, Christopher M. Rouleau & Douglas H. Lowndes

Condensed Matter Sciences Division, Oak Ridge National Laboratory, Oak Ridge, TN 37831, USA

Theoretical predictions – motivated by recent advances in epitaxial engineering – indicate a wealth of complex behaviours arising in superlattices of perovskite-type metal oxides. These include the enhancement of polarization by strain[1,2] and the possibility of asymmetric properties in three-component superlattices[3]. Here we demonstrate unprecedented atomic-scale control of superlattices consisting of barium titanate ($BaTiO_3$), strontium titanate ($SrTiO_3$), and calcium titanate ($CaTiO_3$) by high-pressure pulsed laser deposition on conducting atomically-flat strontium ruthenate ($SrRuO_3$) layers. The strain in $BaTiO_3$ layers is fully maintained as long as the $BaTiO_3$ thickness does not exceed the combined thicknesses of the $CaTiO_3$ and $SrTiO_3$ layers. By preserving full strain and combining heterointerfacial couplings, we find an overall 50% enhancement of the superlattice's global polarization with respect to similarly grown pure $BaTiO_3$, despite the fact that half of the layers in the superlattice are nominally non-ferroelectric. We further show that even superlattices containing only single-unit cell layers of $BaTiO_3$ in a paraelectric matrix remain ferroelectric. Our data reveal that the specific interface structure and local asymmetries play an unexpected role in the polarization enhancement.

Oxide heterostructures with atomically abrupt interfaces, defined by atomically flat surface terraces and single unit-cell steps, now can be grown on well-prepared single-stepped substrates[4-7]. This advance has encouraged theoretical investigations that have led to predictions of new artificial materials[1-3,8-10]. The atomic-scale control of the combining of dissimilar materials is expected to produce striking property enhancements as well as fascinating new combinations of desired properties. Herein we discuss the experimental realization of one of these predictions, the strain-enhancement of ferroelectric polarization. The challenge associated with fabricating such strained structures, i.e. the deliberate and controlled deposition of up to hundreds of individual layers, remains a formidable task, for which the principal technique used has been high-vacuum molecular beam epitaxy (MBE)[5,11]. However, many insulators do not yield the correct oxide stoichiometry or appropriate physical properties (as a result) when grown by MBE. Furthermore, a shortage of electrically conducting oxide substrates and our still-limited understanding of the stability and growth mechanisms of conducting-film electrodes have hindered the electrical characterization of oxide superlattices.

To address these challenges, we have recently shown that atomically-flat, electrically conducting $SrRuO_3$ electrodes can be grown with a surface quality that mimics that of the substrate (Fig. 1a)[7]. Pulsed laser deposition (PLD) has long been regarded as an effective method for synthesizing various oxide heterostructures[12-15], but obtaining atomically sharp interfaces has been difficult in the comparatively high-pressure processes needed to maintain oxygen stoichiometry. Here we demonstrate for the first time the growth by a high-pressure PLD technique of hundreds of individual perovskite layers of barium titanate ($BaTiO_3$), strontium titanate ($SrTiO_3$), and calcium titanate ($CaTiO_3$). These superlattices were grown with layer-by-layer control, yielding *as-grown* samples with compositionally abrupt interfaces, atomically smooth surfaces, and excellent ferroelectric behaviours indicative of oxygen stoichometry. Furthermore, while several earlier studies have utilized two-component $BaTiO_3/SrTiO_3$ structures[16-19]

we focus here on three-component superlattices (TCSs). This breaks the inversion symmetry[3,20] that persists with most two-component superlattices and provides additional freedom in tuning the average lattice parameter by using materials with smaller ($CaTiO_3$) and larger ($BaTiO_3$) unit cell volumes than that of the substrate.

The PLD growth temperature was ~700 ^oC with a relatively high oxygen pressure of 10 mTorr to ensure adequate oxidation. Growth conditions were optimized to require about 200 laser pulses per unit cell; this comparatively low deposition rate[21] allows us to terminate precisely each layer and thus minimize compositional intermixing[22]. Throughout this paper, we denote unit cells of $CaTiO_3$, $SrTiO_3$, and $BaTiO_3$ as C, S, and B, respectively, and define a repeated stacking of z unit cells of $CaTiO_3$ on y unit cells of $BaTiO_3$ on x unit cells of $SrTiO_3$ as "$S_xB_yC_z$", i.e. starting the labelling from the bottom layer. The TCS structures studied include $S_xB_xC_x$ (x = 1, 2, 5, and 10), $S_xB_yC_x$ (x =2 and y = 4, 6, 8), $S_xB_yC_y$ (x = 4 and y = 2) and $S_xB_xC_y$ (x = 2 and y = 4).

Figure 1 illustrates the film quality that results from the optimization of the deposition parameters. Cross-sectional Z-contrast scanning transmission electron microscopy (Z-STEM) shows the compositional abruptness between the strontium ruthenate ($SrRuO_3$) bottom electrode and a subsequently deposited $BaTiO_3$ film (Fig. 1a). In this image, a SrO termination of $SrRuO_3$ can be observed (solid arrow), consistent with RHEED investigations by others[23]. Figure 1b depicts an atomic force microscopy (AFM) image of a $SrRuO_3$ film on a $SrTiO_3$ substrate. The single terrace steps (~0.4 nm in height) observed on this $SrRuO_3$ surface are a direct replica of those observed on the $SrTiO_3$ substrates and thus provide an ideal starting condition for the TCS growth. In fact, we usually observed pronounced oscillations of the RHEED specular spot to persist even when growing superlattices up to 1 micron in thickness (data not shown). As shown in Fig. 1c, an AFM image of the top surface of a 200 nm-thick superlattice ($S_2B_2C_2$) exhibits a surface quality almost identical to that of the

substrate and the $SrRuO_3$ film, again with single unit cell steps (~0.4 nm). A cross sectional Z-contrast image of the corresponding structure in Fig. 1d indeed demonstrates the compositional abruptness of the layers. X-ray scans reveal that the entire structure grows "coherently," i.e. with a single value of the in-plane lattice parameter throughout the entire thickness. The long-range periodicity of this layering is further confirmed by x-ray diffraction (XRD): Figure 1e shows an XRD θ–2θ scan of a $(S_2B_6C_2)_{50}$ superlattice grown on $SrRuO_3$(10 nm)/$SrTiO_3$ exhibiting clear superlattice peaks associated with the periodicity of the structure. Most structures also show a good peak separation between the Cu-Kα_1 and Kα_2 lines (see also the XRD reciprocal space maps below), corresponding to well-defined lattice planes with high crystallinity.

In order to correlate strain and ferroelectric properties, XRD reciprocal space mapping (RSM) is used to quantify the strain state. Figure 2a shows an area-scan through the 114 $BaTiO_3$ peak in reciprocal space of a 200 nm thick $BaTiO_3$ film on a $SrRuO_3$(4 nm)/$SrTiO_3$ substrate. Peaks with identical Q_x values correspond to crystalline material with identical in-plane lattice parameter. Thus the data of Fig. 2a show that the in-plane lattice parameter of the $BaTiO_3$ single film is larger than that of the substrate by about 2.5%, i.e. the interfacial strain resulting from the substrate is largely relaxed (relieved by the formation of defects).

In contrast, interleaving $BaTiO_3$ layers with $SrTiO_3$ and $CaTiO_3$ layers in a superlattice structure can result in a material in which the in-plane lattice parameter is identical to that of the substrate (and thus smaller than in bulk $BaTiO_3$). Figure 2b shows the RSM for a $S_1B_1C_1$ and a $S_2B_2C_2$ structure; perfect in-plane matching in $S_xB_xC_x$ structures was observed even at values of x=10. Such structures are particularly interesting, as they allow us to experimentally test results from calculations[1]. These calculations indicate a strain-enhancement of the ferroelectric polarization in $BaTiO_3$ by about 50% as a consequence of an increase in the tetragonality (resulting from a

decrease of the in-plane lattice parameter). Competing with this strain-enhancement is the effect of the "dilution" of the ferroelectric material in a paraelectric matrix. Density functional calculations on $SrTiO_3/BaTiO_3$ superlattices[1] indicate that the polarization is significantly larger than what would be expected from the $SrTiO_3$ and $BaTiO_3$ volume fractions alone, due to electric-field induced polarization in $SrTiO_3$. Calculations further predict ferroelectricity in superlattices containing only single-unit cell layers of ferroelectric $BaTiO_3$ in an otherwise paraelectric matrix. In addition, even for structures containing single-unit-cell layers of $BaTiO_3$, the numerical results agree remarkably well with those from macroscopic considerations of independent ferroelectric and paraelectric slabs with dielectric constants ε_{FE} and ε_{PE}, respectively. In this electrostatic model, the average polarization is found to be

$$P_{avg} = P_{FE}\cdot[1+(t_{PE}/t_{FE})\cdot(\varepsilon_{FE}/\varepsilon_{PE})]^{-1}, \qquad (1)$$

where P_{FE} is the polarization of the ferroelectric layer, and t_{FE} and t_{PE} are the thickness of ferroelectric and paraelectric layers, respectively.

For our TCSs containing one ferroelectric and two paraelectric components ($SrTiO_3$ with thickness t_{STO} and dielectric constant ε_{STO}, and $CaTiO_3$ with t_{CTO} and ε_{CTO}), the electrostatic considerations (Eq. 1) are easily generalized by letting $t_{PE} = t_{STO} + t_{CTO}$ and $\varepsilon_{PE} = \varepsilon_{STO}\cdot\varepsilon_{CTO}(t_{STO}+t_{CTO}) / (\varepsilon_{STO}\cdot t_{CTO} + \varepsilon_{CTO}\cdot t_{STO})$. Therefore, based on electrostatics alone, the $S_1B_1C_1$ and $S_2B_2C_2$ structures should exhibit identical values of the polarization, while in fact $P_r(S_1B_1C_1) \approx 3.0\ \mu C/cm^2$ and $P_r(S_2B_2C_2) \approx 5.4\ \mu C/cm^2$, indicating that the interfaces play a significant role. Moreover, as expected from previous work on $SrTiO_3/BaTiO_3$ superlattices[17,19], the dielectric constants $\varepsilon(E)$ as determined from $C(V)$ curves at 100 kHz (Fig. 2d) are larger than that of the $BaTiO_3$ film.

Interestingly, increasing the number of neighboring Ba layers results in an increase of the enhancement of the polarization, pointing to the limitations of simple electrostatic considerations (Eq. 1). As illustrated in the schematic drawing of Fig. 4e below, the TiO_6 octahedra (which in the simplest picture are most responsible for the ferroelectric polarization) can be grouped into two classes: those bound on both sides by the same A-site cations (e.g., Ba-surrounded TiO_6) and those forming the interface between $BaTiO_3$, $SrTiO_3$ or $CaTiO_3$ (interfacial TiO_6).

In order to clarify the interplay between strain-enhancement of the polarization and interfacial effects, we modified the number of interfaces and of neighbouring $BaTiO_3$ layers by interleaving identical $SrTiO_3$ and $CaTiO_3$ stackings with different numbers of $BaTiO_3$ layers (while keeping the total thickness fixed). Figures 3a–c show RSMs (nearby the 114 $SrTiO_3$ reflection) of the $S_2B_4C_2$, $S_2B_6C_2$, and $S_2B_8C_2$ superlattices, respectively. A coherent in-plane lattice parameter is obtained only if the $BaTiO_3$ thickness in each superlattice period does not exceed the combined thickness of the $SrTiO_3$ and $CaTiO_3$ layers; consequently, a partial strain relaxation of 0.05% ($S_2B_6C_2$) and 1.21% ($S_2B_8C_2$) is observed in Figs. 3b and c, respectively. The evolution of the in-plane lattice parameter is shown in Fig. 4c as a function of the stacking sequence. In Fig. 4d, we show the polarization for the same structures. Clearly, the strongest polarization enhancement is achieved by the proper balancing between two competing requirements: the $BaTiO_3$ layers must be thick enough to contain a sufficient amount of non-interfacial TiO_6 octahedra, but thin enough to remain fully strained. This produces a maximum polarization for the $S_2B_4C_2$ structure as shown in Fig. 4a. Despite the low volume fraction of 50% $BaTiO_3$, we observe an almost 50% increase in polarization ($P_r \approx 16.5$ μC/cm^2 at 1 MV/cm) over that of the $BaTiO_3$ sample. This polarization is significantly larger than the value of 10.9 μC/cm^2 that would be predicted from electrostatic considerations alone, using bulk values for the effective dielectric constants $\varepsilon_{STO} = 300$, $\varepsilon_{CTO} = 186$, and $\varepsilon_{BTO} = 160$.

The fundamental difference between interfacial cells of $BaTiO_3$ and TiO_6-octahedra in an environment resembling that of bulk $BaTiO_3$ is further illustrated by considering structures of an equal eight-unit cell periodicity but different arrangements, i.e. $S_4B_2C_2$, $S_2B_4C_2$, and $S_2B_2C_4$. All these structures are fully strained, and as pointed out above, the $S_2B_4C_2$ structure shows very strong polarization enhancement. In contrast, the other two samples of this series are characterized by $P_r < 3$ μC/cm^2 (data not shown), slightly less than what would be expected from our $BaTiO_3$ data and the lower $BaTiO_3$ volume fraction (Eq. 1).

The fact that Eq. 1 is insufficient to describe our data for three-component structures but almost perfectly reproduces the calculated behaviour of two-component $BaTiO_3/SrTiO_3$ superlattices points to additional effects that play a role here. One key weakness of applying Eq. 1 to the TCS configuration is the treatment of the $CaTiO_3/SrTiO_3$ bi-layer as a simple dielectric with a passive interface. In reality, local distortions at the $SrTiO_3/CaTiO_3$ interface may also play a role, possibly even inducing a polarization in the neighbouring $SrTiO_3$ cells. Furthermore, for the samples considered here, the environment of the $BaTiO_3$ layers is strongly asymmetric. Considering the theoretically predicted enhancement of the polarization due to breaking of inversion symmetry will therefore be important to understand these materials[3]. A previous report on similar TCS structures observed strong indications of asymmetry in $\varepsilon(E)$, but without ferroelectric hysteresis[11]. In contrast, the samples studied here exhibit strong ferroelectric switching with hysteresis curves both in $P(E)$ and $\varepsilon(E)$. However, asymmetry is observed here even in simple $BaTiO_3$ films. Therefore, we cannot neglect the possible effect of the dissimilar top and bottom electrodes (Pt and $SrRuO_3$, respectively) on the asymmetric behavior. Nevertheless, close inspection of the $\varepsilon(E)$ curves in Fig. 4b shows a varying degree of asymmetry within each individual peak for different stacking sequences. This behavior is not easily explained simply as a

consequence of different electrode materials, but is expected to result from compositionally-broken inversion symmetry[3].

This analysis of atomic-scale precision TCS structures thus leads to two significant observations: First, the use of three-component materials, as dictated by the need for near-perfect lattice matching to the substrate, reveals the subtle effects of a non-inversion symmetric environment and the role of a large number of coupled heterointerfaces. Second, these structures have allowed for the first time the experimental verification of theoretical predictions of strain-enhanced ferroelectric polarization of $BaTiO_3$, even in structures containing a relatively small volume-fraction of $BaTiO_3$. These results, together with the advance in pulsed laser deposition reported here, illustrate how enhancements of material properties – needed for applications in sensors, high-*k* dielectrics, and piezoelectric and ferroelectric devices – can be produced.

Methods

Before growing the TCSs, epitaxial $SrRuO_3$ films (4–16 nm in thickness) were grown by PLD on single-stepped (001) $SrTiO_3$ substrates using a KrF excimer laser (λ = 248 nm) at 700 °C in 100 mTorr O_2. The TCSs were also grown by PLD at ~700 ^{o}C in 10 mTorr O_2 using sintered stoichiometric $CaTiO_3$ and $BaTiO_3$ targets, and a single-crystal $SrTiO_3$ target. We have previously shown that this combination of pressure and temperature lies within the stability range for our $SrRuO_3$ films[7]. In addition, the use of $CaTiO_3$ in the superlattice enhances the compressive strain, allows the average in-plane lattice parameter of the superlattice to match that of the substrate, and induces a wider range of elastic behaviour at the interface with $BaTiO_3$. The laser repetition rate and laser fluence were kept at 10 Hz and 2 J/cm^2, respectively. The deposition of each individual unit cell was monitored via the intensity oscillations of the specular spot in RHEED pattern. The topmost layer was capped by one or two unit-cells of $SrTiO_3$ and

the final thickness of all superlattices was fixed at 200 nm. For the electrical characterization, sputtered Pt top electrodes (100 μm in diameter) were used together with the conducting $SrRuO_3$ bottom electrode.

Figure captions

Figure 1 Atomic-scale flatness and compositional abruptness in surfaces and interfaces of conducting $SrRuO_3$ and artificial superlattices. **a**, Cross-sectional Z-contrast image of interface between $BaTiO_3$ and $SrRuO_3$ films, indicated by the black arrow. **b**, AFM topographic images (image size: 4×5 μm^2) with single terrace steps (~0.4 nm) of $SrRuO_3$ and **c** of a 200 nm thick $S_2B_2C_2$ superlattice. A RHEED pattern in the inset in Fig. 1**c** also confirms the exceptionally smooth surface. **d**, Cross-sectional Z-contrast image of compositionally abrupt interfaces in $S_2B_2C_2$; the schematic shows its atomic structure. **e**, XRD θ–2θ scan of a $S_2B_6C_2$ confirming the long-range periodicity and high crystallinity. The STO 001 and 002 peaks are from the $SrTiO_3$ substrate.

Figure 2 Strain states of a $BaTiO_3$ single film and superlattices on $SrRuO_3/SrTiO_3$ substrates and their ferroelectric properties. **a, b,** XRD-RSMs of a $BaTiO_3$ thin film and of a $S_2B_2C_2$ superlattice, respectively (Q_x and Q_y in units of $1/d$). A RSM of $S_1B_1C_1$ is also shown in the inset of **b**, showing clearly peaks from the Cu-Kα_1 (†) and Cu-Kα_2 (*) radiations. The solid red vertical lines mark the 114 $SrTiO_3$ Cu-Kα_1 peak position, and the dotted red line that of $BaTiO_3$. Peaks marked with black and red arrows correspond to reflections from the $SrTiO_3$ substrate, respectively, and from the film or superlattice layer and satellites. **c, d,** $P(E)$ at 100 Hz and $\varepsilon(E)$ hysteresis loops at 100 kHz, from 200 nm thick $BaTiO_3$ (black curves), $S_1B_1C_1$ (red) and $S_2B_2C_2$ (green).

Figure 3 Evolution of the in-plane strain with changes in the thickness of $BaTiO_3$ layers for fixed thickness of $SrTiO_3$ and $CaTiO_3$. **a, b, c,** XRD-RSMs of $S_2B_4C_2$, $S_2B_6C_2$ and $S_2B_8C_2$ superlattices, respectively, showing a gradual increase in the in-plane lattice parameter. (Solid and dotted red vertical lines mark the peak(s) of the substrate and superlattice, respectively.) The RSMs are

recorded around the 114 $SrTiO_3$ reflection. SRO in **a** indicated by the blue arrow stands for $SrRuO_3$ reflected from a relatively thick film (16 nm).

Figure 4 Polarization enhancement, changes in asymmetry, and evolution of strain in TCS structures. **a,** $P(E)$ curves of a $S_2B_4C_2$ ($P_r \approx 16.5$ μC/cm^2) and a $S_{10}B_{10}C_{10}$ ($P_r \approx 3.5$ μC/cm^2) at 1000 kV/cm. [Note that this electric field is higher than that applied to measure the polarization of the $BaTiO_3$ film, whose polarization is near saturation at 400 kV/cm, while the $S_2B_4C_2$ requires a higher electric field (~700 kV/cm)]. **b,** $\varepsilon(E)$ curves of $S_2B_4C_2$ (black line), $S_2B_6C_2$ (red line), $S_4B_2C_2$ (green line) and $S_{10}B_{10}C_{10}$ (blue line) showing differing degrees of asymmetry. **c,** In-plane (open squares) and out-of-plane (solid squares) lattice parameters of various superlattices. *c*' corresponds to the supercell *c* divided by the number of constituent perovskites in a supercell. **d,** P_r values from $E = \pm 750$ kV/cm loops. The partially relaxed $S_2B_8C_2$ structure was measured with E = ± 650 kV/cm due to its lower breakdown strength. **e,** Schematics of supercells showing the different local environments possible for the TiO_6-octahedra (bound by the same or different A-site cations). Heterointerfacial TiO_6 octahedra are highlighted in grey colour and indicated by solid black arrows.

References

1. Neaton, J. B. & Rabe, K. M. Theory of polarization enhancement in epitaxial $BaTiO_3/SrTiO_3$ superlattices. *Appl. Phys. Lett*. **82**, 1586–1588 (2003).
2. Pertsev, N. A., Tagantsev, A. K. & Setter, N. Phase transitions and strain-induced ferroelectricity in $SrTiO_3$ epitaxial thin films. *Phys. Rev. B* **61,** R825-829 (2000).
3. Sai, N., Meyer, B. & Vanderbilt, D. Compositional inversion symmetry breaking in ferroelectric perovskites. *Phys. Rev. Lett.* **84,** 5636–5639 (2000).
4. Kawasaki, M. *et al*. *Science* **266**, 1540–1542 (1994).
5. Schlom, D. G. *et al*. Oxide nano-engineering using MBE. *Mater. Sci. Eng. B* **87,** 282–291 (2001).
6. Yamada, H. *et al*. Engineered interface of magnetic oxides. *Science* **305,** 646–648 (2004).
7. Lee, H.N., Christen, H. M., Chisholm, M. F., Rouleau, C. M. & Lowndes, D. H. Thermal stability of epitaxial $SrRuO_3$ films as a function of oxygen pressure. *Appl. Phys. Lett.* **84,** 4107–4109 (2004).
8. Okamoto, S. & Millis, A. J. Electronic reconstruction at an interface between a Mott insulator and a band insulator. *Nature* **428,** 630–633 (2004).
9. Junquera, J. & Ghosez, P. Critical thickness for ferroelectricity in perovskite ultrathin films. *Nature* **422,** 506–509 (2003).
10. Glinchuk, M. D. & Morozovska, A. N. The internal electric field originating from the mismatch effect and its influence on ferroelectric thin film properties. *J. Phys.: Condens. Matter* **16** 3517–3531 (2004).
11. Warusawithana, M. P., Colla, E. V., Eckstein, J. N. & Weissman, M. B. Artificial dielectric superlattices with broken inversion symmetry. *Phys. Rev. Lett.* **90,** 36802 (2003).

12. Lee, H. N., Hesse, D., Zakharov, N. & Gösele, U. Ferroelectric $Bi_{3.25}La_{0.75}Ti_3O_{12}$ films of uniform *a*-axis orientation on silicon substrates. *Science* **296,** 2006–2009 (2002).

13. Christen, H. M. *et al*. An improved continuous compositional-spread technique based on pulsed-laser deposition and applicable to large substrate areas. *Rev. Sci. Instrum*. **74,** 4058–4062 (2003).

14. Zheng, H. *et al*. Multiferroic $BaTiO_3$-$CoFe_2O_4$ nanostructures. *Science* **303**, 661–663 (2004).

15. Norton, D. P. Synthesis and properties of epitaxial electronic oxide thin-film materials. *Mater. Sci. Eng. R* **43,** 139–247 (2004).

16. Tabata, H., Tanaka, H. & Kawai, T. Formation of artificial $BaTiO_3/SrTiO_3$ superlattices using pulsed laser deposition and their dielectric properties. *Appl. Phys. Lett*. **65,** 1970–1972 (1994).

17. O'Neill, D. Bowman, R. M. & Gregg, J. M. Dielectric enhancement and Maxwell-Wagner effects in ferroelectric superlattice structures. *Appl. Phys. Lett.* **77,** 1520–1522 (2000).

18. Shimuta, T. *et al*. Enhancement of remanent polarization in epitaxial $BaTiO_3/SrTiO_3$ superlattices with asymmetric structure. *J. Appl. Phys.* **91,** 2290–2294 (2002).

19. Kim, J. *et al*. Large nonlinear dielectric properties of artificial $BaTiO_3/SrTiO_3$ superlattices. *Appl. Phys. Lett.* **80,** 3581–3583 (2002).

20. Ogawa, Y. *et al.* Nonlinear magneto-optical Kerr rotation of an oxide superlattice with artificially broken symmetry. *Phys. Rev. Lett*. **90**, 217403 (2003).

21. Muller, D. A. Nakagawa, N, Ohtomo, A, Grazul, J. L. & Hwang, H. Y. Atomic-scale imaging of nanoengineered oxygen vacancy profiles in $SrTiO_3$. *Nature* **430,** 657–661 (2004).

22. Lee, H. N. *et al*. Compositionally asymmetric tri-color superlattices grown by pulsed laser deposition. *Mater. Res. Soc. Symp. Proc.* **784,** C3.24 (2004).

23. Rijnders, G., Blank, D. H. A., Choi, J. & Eom, C. B. Enhanced surface diffusion through termination conversion during epitaxial $SrRuO_3$ growth. *Appl. Phys. Lett.* **84,** 505–507 (2004).

Acknowledgements This work was supported by the U.S. Department of Energy under contract with the Oak Ridge National Laboratory, managed by UT-Battelle, LLC, as part of a BES NSET initiative on Nanoscale Cooperative Phenomena and of the LDRD program.

Correspondence and requests for materials should be addressed to H.N.L. (e-mail: hnlee@ornl.gov).

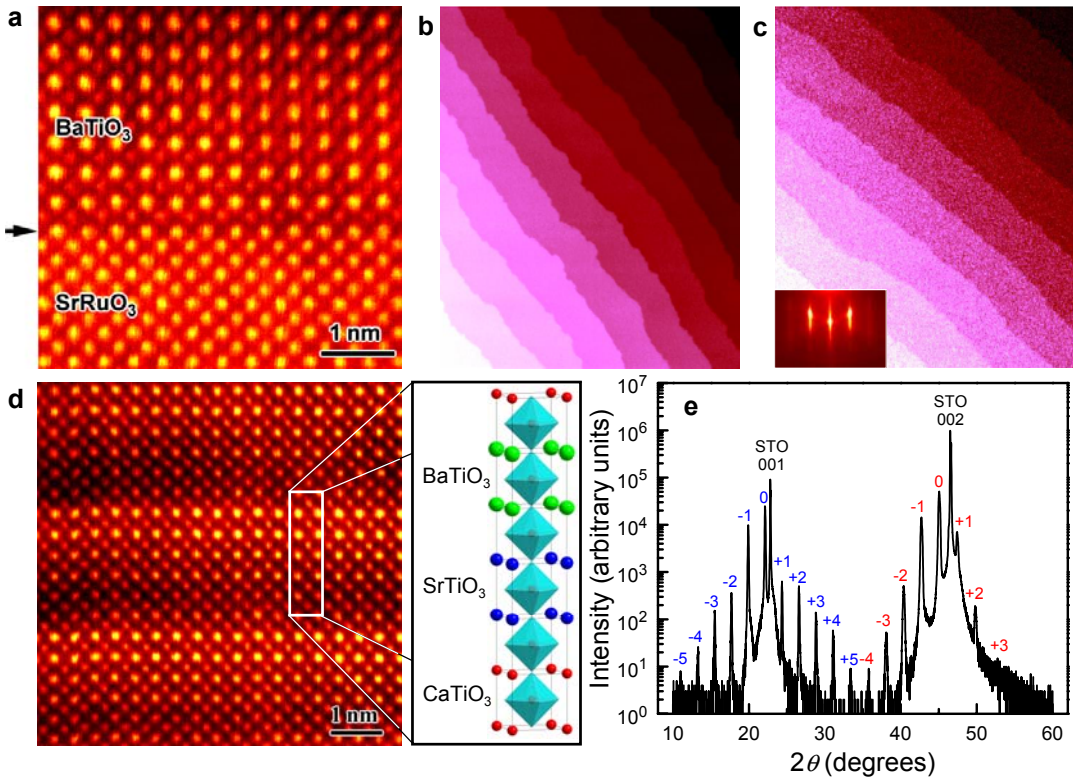

Fig. 1 H. N. Lee *et al.*
(MS# 2004-09-24271)

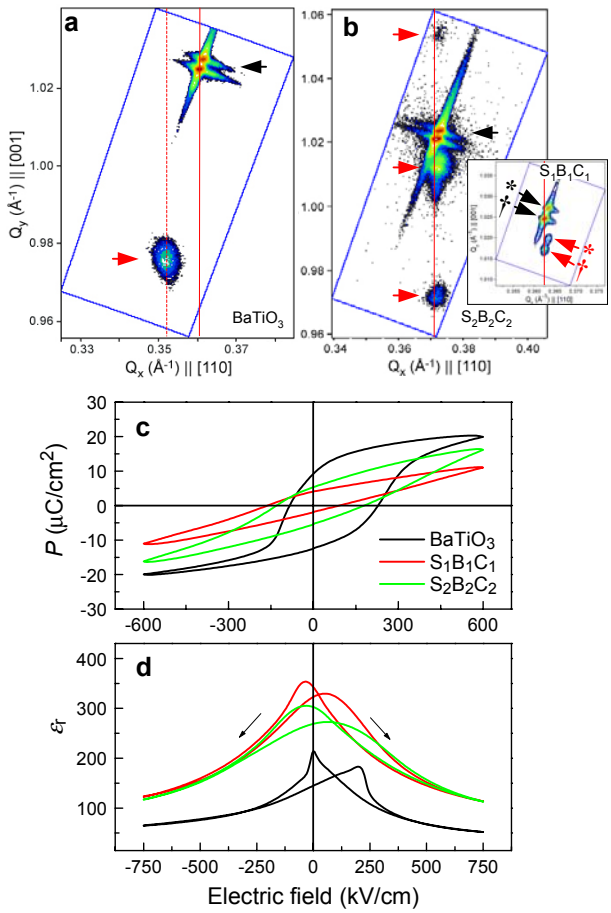

Fig. 2 H. N. Lee *et al.*
(MS# 2004-09-24271)

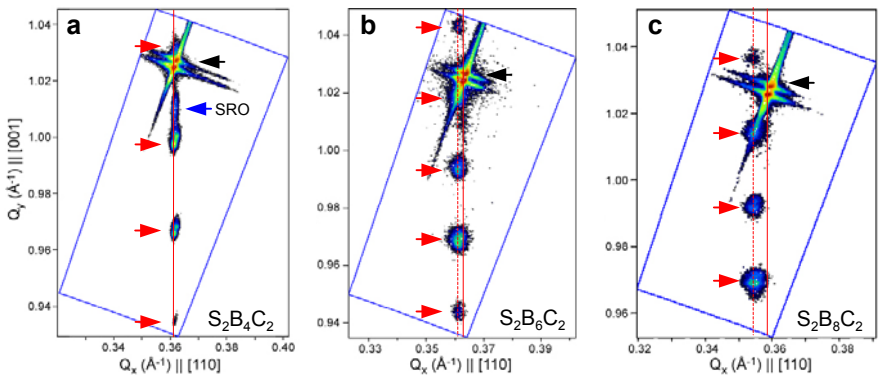

Fig. 3 H. N. Lee *et al.*
(MS# 2004-09-24271)

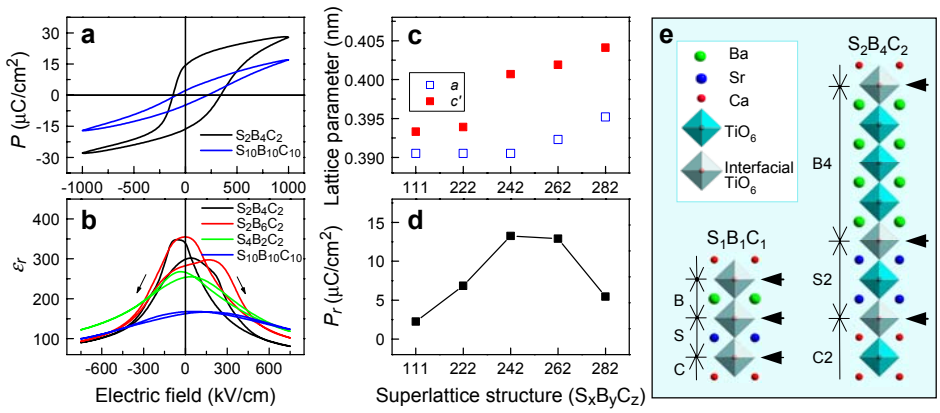

Fig. 4 H. N. Lee *et al.*
(MS# 2004-09-24271)